ChemComm

Reduction of CS2 to an Ethanetetrathiolate by a Hydride-Bridged Uranium–Iridium Heterobimetallic Complex

Journal:	*ChemComm*
Manuscript ID	CC-COM-05-2024-002482.R2
Article Type:	Communication

COMMUNICATION

Reduction of CS_2 to an Ethanetetrathiolate by a Hydride-Bridged Uranium–Iridium Heterobimetallic Complex

Received 00th January 20xx,
Accepted 00th January 20xx

DOI: 10.1039/x0xx00000x

Christopher Z. Ye,[a,b] Iker Del Rosal,[c] Erik T. Ouellette,[a,b] Stephan Hohloch,[d] Laurent Maron,[c] Clément Camp*[e], and John Arnold*[a,b]

We report the synthesis of a heterobimetallic U(III)–Ir species which reacts with CS_2 to form the novel ethanetetrathiolate fragment *via* hydride insertion and C–C coupling. Computational studies suggest the formation of a radical intermediate which may couple with another equivalent to form the final product.

Transition metal (TM) hydrides play important roles in organometallic chemistry and catalysis, being implicated as intermediates in numerous catalytic reactions, such as olefin hydrofunctionalization,[1] redox electrocatalysis,[2] and small molecule reduction/activation.[3,4] TM polyhydrides appear well-suited to forming heterobimetallic complexes, typically consisting of an electron-rich transition metal hydride in concert with an electron-deficient Lewis acid; some of these complexes are capable of novel cooperative reactivity. Main-group Lewis acids and cationic coinage metals in particular have been shown to be competent partners for electron-rich transition metal hydrides, enabling transformations including carbonyl reduction, H_2 activation, and olefin polymerization.[5,6]

Given the well-established Lewis acidity of the actinides (An),[7] it is surprising that relatively few efforts to pair them with transition metal hydrides have been reported, though An borohydrides and aluminohydrides are well known.[8–11] Ephritikhine synthesized the first hydride-bridged An–TM complexes with a series of U–Re species; no reactivity was reported,[12–14] and the field has laid dormant in the subsequent years. We recently demonstrated that salt metathesis reactions with $K[Cp^*IrH_3]$ and actinide halide starting materials led to the hydride-supported U(IV)–Ir species $U\{(\mu\text{-}H)_3IrCp^*\}_4$ (**A**).[15] As with the U–Re complexes above, we found no evidence for reactivity towards small molecules such as alkenes, CO_2, and CS_2. This was surprising to us, given the documented ability of Lewis acid-coupled iridium hydrides to promote reactions such as ketone hydrogenation,[16] H/D exchange,[17–21] cleavage of heteroallenes,[22] and alkene dehydrogenation.[23]

In attempts to increase the reactivity of An–Ir polyhydride species, we first aimed to synthesize a heterobimetallic system with only one metal–metal interaction, which would allow for a more accessible actinide center; second, we sought a potentially more reactive U(III) center.[24] CS_2 reduction is well-precedented for U(III) complexes, producing numerous anionic fragments such as CS_2^{2-}, CS_3^{2-}, $C_2S_4^{2-}$, $C_2S_4^{4-}$, and $C_3S_5^{2-}$ (Figure 1a).[25–33] On the other hand, the insertion of CS_2 into metal-hydride bonds is documented for transition metal systems, resulting in the formation of metal dithioformate complexes (Fig. 1b).[34–38] Here, we report the use of the U(III) metallocene $(Cp^{iPr4})_2UI$[39] (Cp^{iPr4} = tetra(isopropyl)cyclopentadienyl) to support a reactive U(III)–Ir complex which combines the reductive C–C coupling chemistry of U(III) with the insertion chemistry of transition metal hydrides, resulting in a novel bridging ethanetetrathiolate fragment (Figure 1c).

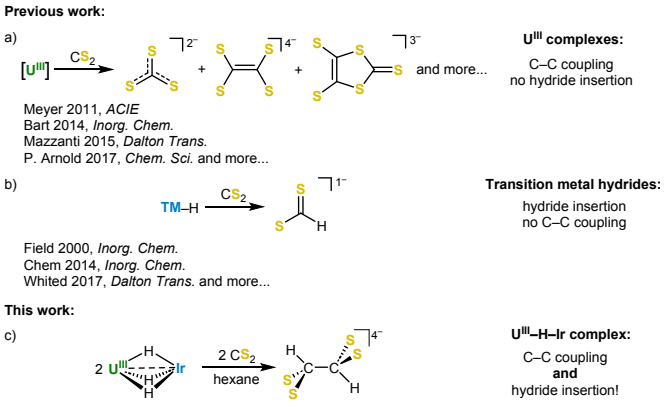

Figure 1 Previously reported reactivity of CS_2 with U(III) species (a) and transition metal hydrides (b), compared to the U(III)–Ir polyhydride in this work (c).

[a] *Department of Chemistry, University of California, Berkeley, California 94720, USA. E-mail: arnold@berkeley.edu*
[b] *Chemical Sciences Division, Lawrence Berkeley National Laboratory, Berkeley, California 94720, USA*
[c] *Université de Toulouse, CNRS, INSA, UPS, UMR 5215, LPCNO, 135 Avenue de Rangueil, F-31077 Toulouse, France.*
[d] *University of Paderborn, Warburger Straße 100, 33098 Paderborn, Germany.*
[e] *Laboratory of Catalysis, Polymerization, Processes and Materials (CP2M UMR 5128) CNRS, Universite Claude Bernard Lyon 1, CPE-Lyon, Institut de Chimie de Lyon, 43 Bvd du 11 Novembre 1918, 69616 Villeurbanne, France. E-mail: clement.camp@univ-lyon1.fr*
Electronic Supplementary Information (ESI) available: Experimental procedure and additional characterization data. See DOI: 10.1039/x0xx00000x

Equimolar amounts of K[Cp*IrH$_3$] and (Cp^{iPr4})$_2$UI were combined as THF solutions at room temperature to yield the U(III) iridate trihydride (Cp^{iPr4})$_2$U(μ-H)$_3$IrCp* (**1**) after two hours (Scheme 1). Compound **1** is highly soluble in nonpolar solvents, requiring the cooling of concentrated solutions in hexamethyldisiloxane (HMDSO) to –40 °C to isolate solid product as dark green crystals in 51% yield. The influence of the paramagnetic U(III) center is clear in the ^{1}H NMR spectrum; it contains only two sharp resonances. The first is assigned to the iridium-bound Cp* ligand at 4.41 ppm, slightly upfield relative to the signal of tetrairidate **A** at 4.98 ppm.[15] The second appears at 0.12 ppm and corresponds to 0.5 equivalents of co-crystallized HMDSO, as observed in the crystal structure (see below). Two of the remaining broad resonances, at 6.25 ppm and –6.55 ppm, each integrate to ca. 12 protons and are tentatively assigned to isopropyl methyl groups of the Cp^{iPr4} ligands. A third, less intense resonance is located at –31.0 ppm, but cannot be assigned with confidence to either the bridging hydrides or the Cp^{iPr4} ligands. The IR spectrum of **1** contains a strong hydride stretch at 1955 cm^{-1} with a shoulder at 2033 cm^{-1}, comparable to the hydride stretch of 1951 cm^{-1} found in **A**.[15]

Complex **1** crystallizes in the space group $P\bar{1}$ with 0.5 equivalents of HMDSO. Unlike many previously isolated hydride-supported An–TM complexes,[15] the hydrides in **1** were located and refined, though the presence of nearby heavy metal centers increases the uncertainty of these measurements. (Figure 2). Given the monoanionic nature of Cp*IrH$_3^-$,[15,22,18,40] the structure is consistent with a U(III) product with two anionic Cp^{iPr4-} ligands in addition to the Cp*IrH$_3^-$ moiety. The U–Ir distance of 3.0308(3) Å is longer than the average U–Ir distance of 2.954(1) Å in **A**, which is unsurprising given the larger size of the U(III) ion in comparison to U(IV). The Ir–H and U–H bond lengths average 1.52(5) Å and 2.44(5) Å, respectively. The highly linear U–Ir–Cp*$_{centroid}$ angle of 176.56(6)° is consistent with three bridging hydrides, as observed in numerous multimetallic complexes with Cp*IrH$_3^-$ moieties.[15,41–43]

With this heterobimetallic U(III)–Ir species in hand, we began to probe whether it was more reactive to small molecules than the U(IV) complex **A**. Upon addition of 1 equivalent of CS_2 to a hexane solution of **1** at room temperature, there was a rapid color change from dark green to red. Cooling the red solution to –40 °C yielded red crystals of the ethanetetrathiolate dimeric complex **2** after 24 hours (Scheme 1). These red crystals exhibited poor solubility in benzene and THF, which in conjunction with the paramagnetism of the compound made assignment of the ^{1}H NMR spectrum unfeasible. IR spectroscopy reveals several bridging hydride stretches at 2040, 1958, and 1915 cm^{-1} for **2**, shifted slightly higher in frequency relative to those of **1**.

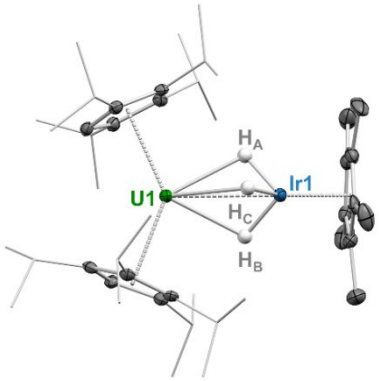

Figure 2 Solid-state molecular structure of **1**. Ellipsoids are drawn at the 50% probability level. Non-hydride hydrogen atoms have been omitted and isopropyl groups have been wireframed for clarity. Selected bond distances (Å) and angles (°): U1–Ir1 3.0308(3), U1–Cp^{iPr4}(cent) 2.5233(3)/2.5387(3), U1–H$_A$ 2.42(5), U1–H$_B$ 2.43(4), U1–H$_C$ 2.46(4), Ir1–H$_A$ 1.47(5), Ir1–H$_B$ 1.54(5), Ir1–H$_C$ 1.51(4), U1–Ir1–Cp*$_{cent.}$ 176.56(6).

Complex **2** crystallizes with one equivalent of *n*-hexane in the space group *C*2/*c*, with half of the molecule generated around a C_2 axis perpendicular to the central C–C bond (Figure 3). The U–Ir distance is significantly lengthened in **2** compared to **1**, at 3.1382(6) Å. The average metal hydride distances are within error of those found for **2**, at 2.47(7) Å (U–H) and 1.56(6) Å (Ir–H). The U–S bond is significantly shorter for the non-bridging sulfur atom compared to the U–S–Ir bridging atom, at 2.6618(13) Å and 2.8204(13) Å, respectively, with a shorter Ir–S bond length of 2.3585(14) Å. The U–S bond lengths fall between the average bond lengths reported for the ethenetetrathiolate complexes [Na(DME)$_3$]$_2$[{((Ad ArO)$_3$N)U}$_2$(μ-C$_2$S$_4$)] (2.951(1) Å) and [{(η^5-1,3-(Me$_3$Si)$_2$C$_5$H$_3$)$_2$U}(μ-C$_2$S$_4$)] (2.633(2) Å).[26,33] The carbon atoms in the $C_2S_4H_2^{4-}$ moiety have near-tetrahedral geometries (τ_4 = 0.96, with α = 113.38(15)°, β = 112(3)°), and the C–C bond length (1.543(8) Å) is that of a C–C single bond.

Each molecule of CS_2, therefore, has been reduced by three electrons in order to form the $C_2S_4H_2^{4-}$ moiety. Two electrons originate from the hydride bond into which CS_2 inserts, while the third is transferred from the U(III) center of **1**, which oxidizes to U(IV) in **2**. This is further corroborated by the UV-vis/NIR spectra of **1** and **2** (Figure S1). The spectrum of complex **1** contains higher intensity, broader NIR absorption features, in line with a U(III) center, compared to the numerous sharp, lower intensity features indicative of a U(IV) species found in the spectrum of **2**.[44,45] The iridium oxidation state remains unchanged, with a bridging hydride replaced with a bridging sulfide.

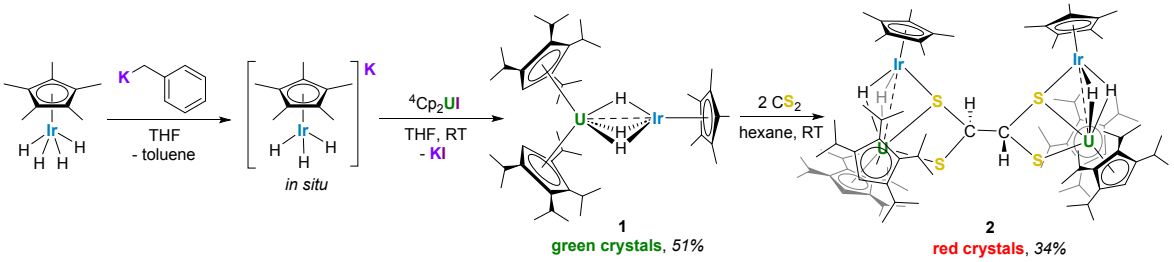

Scheme 1 Synthesis of (Cp^{iPr4})$_2$U(μ-H)$_3$IrCp* (**1**) and subsequent reactivity with CS_2 to form **2**.

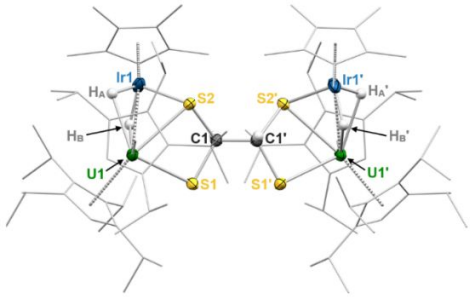

Figure 3 ORTEP diagram of **2**, with ellipsoids drawn at the 50% probability level. Hydrogen atoms of the Cp* and ^{iPr4}Cp ligands have been eliminated, and the ligands have been wireframed for clarity. Selected bond distances (Å) and angles (°): U1–Ir1 3.1382(6), U1–H_A 2.41(6), U1–H_B 2.51(8), Ir1–H_A 1.59(6), Ir1–H_B 1.52(2), U1–S1 2.6618(12), U1–S2 2.8204(12), Ir1–S2 2.3585(12), C1–C1^i 1.542(9), S1–C1–S2 107.3(2).

Additions of CO_2 were investigated for similar reactivity, but the only metal-containing species observed was Cp*IrH_2(CO), a CO_2 cleavage product observed in several other systems.[22]

Calculations were carried out at the DFT level (B3PW91 functional including solvent and dispersion). Three different spin states (Table S2) were considered for complex **1**; a quartet ground state was found to be lowest in energy, while the doublet and sextet are significantly higher (16.0 and 61.4 kcal/mol, respectively). This quartet spin state is in line with the presence of a U(III) center and is corroborated by the unpaired spin density plot (Figure S8). The optimized geometry of complex **1** compares well with experiment; among others, the U–Ir distance is well-reproduced (3.07 Å vs. 3.03 Å experimentally) and the U–H and Ir–H distances are also correctly described (see Figure S11 in ESI).

The mechanism of the formation of **2** from **1** was investigated as well (Figure 4). The reaction begins by the CS_2 insertion into the U–H–Ir three-center bond with a low activation barrier (6.3 kcal/mol). At the transition state (TS), one sulfur atom binds to uranium to allow nucleophilic assistance for CS_2 bending as well as disruption of the U–H interaction. This forms an empty orbital at the carbon atom that is used to abstract the hydride from iridium, yielding a thioformate intermediate (–6.3 kcal/mol) that readily isomerizes by coordinating the second sulfur to both uranium and iridium (–30.2 kcal/mol). Interestingly, this intermediate (**Int1**) displays radical character at carbon (Figure S8) although it is still a U(III) complex in a quartet ground state. This prompted us to investigate the radical coupling between two of these intermediates to form **2** (Figure 4). A low-lying radical coupling TS was found (Figure 4) with an associated barrier of 11.5 kcal/mol. This barrier height is expected for a radical coupling, which must be rapid. Following the intrinsic reaction coordinate, it yields complex **2** whose formation is exothermic by 99.8 kcal/mol. The optimized geometry of **2** (Figure S10) compares well to experiment. In particular, the U–S distances are correctly reproduced (2.67 Å (non-bridging) and 2.84 Å (bridging) vs. 2.66 Å and 2.82 Å experimentally) as well as the short Ir–S distance (2.38 Å vs. 2.36 Å). As with **1**, three different spin states were computed, with the lowest energy found for the quintet state. The unpaired spin density plot (Figure S9) clearly shows the presence of two U(IV) centers in complex **2**.

In conclusion, the heterobimetallic U–Ir trihydride **1** reveals unprecendented reactivity by synergistically combining uranium-driven reductive C–C coupling with the hydride insertion typical of transition metals. This results in the conversion of CS_2 to the novel $C_2S_4H_2^{4-}$ fragment, highlighting the potential for new reactivity mediated by actinide/transition metal hydride species. This could open new avenues in small molecule activation and catalysis, enabling both electron and hydride transfer processes within a single complex.

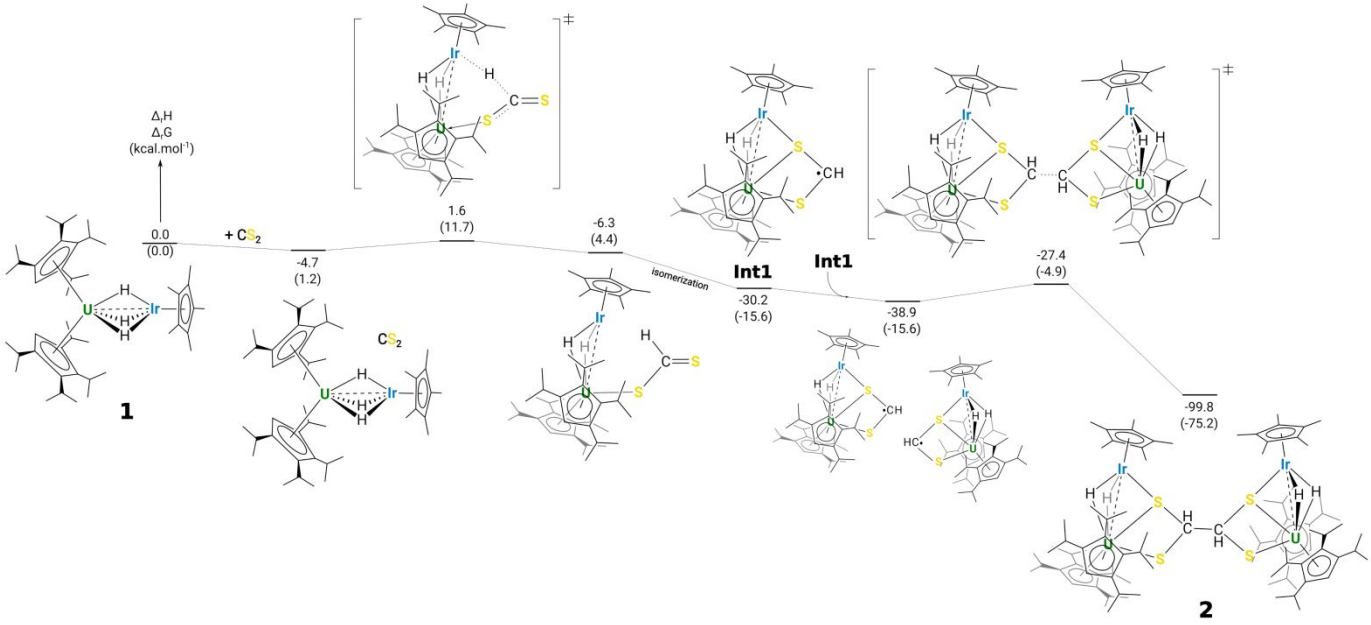

Figure 4 Computed enthalpy (Gibbs free energy in parentheses) profile for the formation of **2** from complex **1**. Energies are given in kcal/mol.

Data Availability Statement

The experimental and computational data associated with this article are provided in the ESI.

Author Contributions

C. Z. Ye conducted the synthetic experimental work. E. T. Ouellette recorded and interpreted the XRD data. I. Del Rosal and L. Maron performed and interpreted the computational studies. S. Hohloch provided the Cp^{4iPr} ligand. C. Z. Ye drafted the original version of the manuscript. J. Arnold, C. Camp conceptualized the research by securing funding and administered the project. J. Arnold, C. Camp, and L. Maron supervised the work, interpreted the data, revised, and subsequently edited the manuscript. All authors have read and agreed to the published version of the manuscript.

References

1 S. W. M. Crossley, C. Obradors, R. M. Martinez and R. A. Shenvi, *Chem. Rev.*, 2016, **116**, 8912–9000.
2 N. A. Eberhardt and H. Guan, *Chem. Rev.*, 2016, **116**, 8373–8426.
3 M. A. Esteruelas and L. A. Oro, *Chem. Rev.*, 1998, **98**, 577–588.
4 A. J. Jordan, G. Lalic and J. P. Sadighi, *Chem. Rev.*, 2016, **116**, 8318–8372.
5 A. Maity and T. S. Teets, *Chem. Rev.*, 2016, **116**, 8873–8911.
6 A. Albinati and L. M. Venanzi, *Coordination Chemistry Reviews*, 2000, **200–202**, 687–715.
7 N. Kaltsoyannis, P. J. Hay, J. Li, J.-P. Blaudeau and B. E. Bursten, in *The Chemistry of the Actinide and Transactinide Elements*, eds. L. R. Morss, N. M. Edelstein and J. Fuger, Springer Dordrecht, 2011.
8 M. Ephritikhine, *Chem. Rev.*, 1997, **97**, 2193–2242.
9 A. C. Dunbar, J. C. Wright, D. J. Grant and G. S. Girolami, *Inorg. Chem.*, 2021, **60**, 12489–12497.
10 A. B. Altman, A. C. Brown, G. Rao, T. D. Lohrey, R. D. Britt, L. Maron, S. G. Minasian, D. K. Shuh and J. Arnold, *Chem. Sci.*, 2018, **9**, 4317–4324.
11 R. J. Ward, P. Rungthanaphatsophon, P. Huang, S. P. Kelley and J. R. Walensky, *Chem. Sci.*, 2023, **14**, 12255–12263.
12 D. Baudry and M. Ephritikhine, *Journal of Organometallic Chemistry*, 1986, **311**, 189–192.
13 S. M. Cendrowski-Guillaume, M. Lance, M. Nierlich, J. Vigner and M. Ephritikhine, *J. Chem. Soc., Chem. Commun.*, 1994, 1655–1656.
14 S. M. Cendrowski-Guillaume and M. Ephritikhine, *J. Chem. Soc., Dalton Trans.*, 1996, 1487–1491.
15 C. Z. Ye, I. D. Rosal, M. A. Boreen, E. T. Ouellette, D. R. Russo, L. Maron, J. Arnold and C. Camp, *Chem. Sci.*, 2023, **14**, 861–868.
16 J. M. Hayes, E. Deydier, G. Ujaque, A. Lledós, R. Malacea-Kabbara, E. Manoury, S. Vincendeau and R. Poli, *ACS Catal.*, 2015, **5**, 4368–4376.
17 M. Oishi, M. Kino, M. Saso, M. Oshima and H. Suzuki, *Organometallics*, 2012, **31**, 4658–4661.
18 M. Oishi, M. Oshima and H. Suzuki, *Inorg. Chem.*, 2014, **53**, 6634–6654.
19 M. R. Kita and A. J. M. Miller, *J. Am. Chem. Soc.*, 2014, **136**, 14519–14529.
20 S. Lassalle, R. Jabbour, P. Schiltz, P. Berruyer, T. K. Todorova, L. Veyre, D. Gajan, A. Lesage, C. Thieuleux and C. Camp, *J. Am. Chem. Soc.*, 2019, **141**, 19321–19335.
21 A. V. Pichugov, L. Escomel, S. Lassalle, J. Petit, R. Jabbour, D. Gajan, L. Veyre, E. Fonda, A. Lesage, C. Thieuleux and C. Camp, *Angewandte Chemie International Edition*, 2024, **63**, e202400992.
22 L. Escomel, I. Del Rosal, L. Maron, E. Jeanneau, L. Veyre, C. Thieuleux and C. Camp, *J. Am. Chem. Soc.*, 2021, **143**, 4844–4856.
23 S. Morisako, S. Watanabe, S. Ikemoto, S. Muratsugu, M. Tada and M. Yamashita, *Angewandte Chemie International Edition*, 2019, **58**, 15031–15035.
24 M. A. Boreen and J. Arnold, *Dalton Trans.*, 2020, **49**, 15124–15138.
25 J. G. Brennan, R. A. Andersen and A. Zalkin, *Inorg. Chem.*, 1986, **25**, 1756–1760.
26 O. P. Lam, F. W. Heinemann and K. Meyer, *Angewandte Chemie International Edition*, 2011, **50**, 5965–5968.
27 V. Mougel, C. Camp, J. Pécaut, C. Copéret, L. Maron, C. E. Kefalidis and M. Mazzanti, *Angewandte Chemie International Edition*, 2012, **51**, 12280–12284.
28 E. M. Matson, A. T. Breshears, J. J. Kiernicki, B. S. Newell, P. E. Fanwick, M. P. Shores, J. R. Walensky and S. C. Bart, *Inorg. Chem.*, 2014, **53**, 12977–12985.
29 C. Camp, O. Cooper, J. Andrez, J. Pécaut and M. Mazzanti, *Dalton Trans.*, 2015, **44**, 2650–2656.
30 P. L. Arnold, C. J. Stevens, N. L. Bell, R. M. Lord, J. M. Goldberg, G. S. Nichol and J. B. Love, *Chem. Sci.*, 2017, **8**, 3609–3617.
31 R. J. Ward, S. P. Kelley, W. W. Lukens and J. R. Walensky, *Organometallics*, 2022, **41**, 1579–1585.
32 S. Wang, D. Wang, T. Li, Y. Heng, G. Hou, G. Zi and M. D. Walter, *Organometallics*, 2022, **41**, 1543–1557.
33 Y. Heng, T. Li, D. Wang, G. Hou, G. Zi and M. D. Walter, *Organometallics*, 2023, **42**, 91–113.
34 L. D. Field, E. T. Lawrenz, W. J. Shaw and P. Turner, *Inorg. Chem.*, 2000, **39**, 5632–5638.
35 J. Huang, J. Chen, H. Gao and L. Chen, *Inorg. Chem.*, 2014, **53**, 9570–9580.
36 M. T. Whited, J. Zhang, S. Ma, B. D. Nguyen and D. E. Janzen, *Dalton Trans.*, 2017, **46**, 14757–14761.
37 M. Rauch and G. Parkin, *Dalton Trans.*, 2018, **47**, 12596–12605.
38 J. P. Lanorio and B. J. Frost, *Inorganica Chimica Acta*, 2019, **498**, 119138.
39 M. A. Boreen, D. J. Lussier, B. A. Skeel, T. D. Lohrey, F. A. Watt, D. K. Shuh, J. R. Long, S. Hohloch and J. Arnold, *Inorg. Chem.*, 2019, **58**, 16629–16641.
40 L. Escomel, N. Soulé, E. Robin, I. Del Rosal, L. Maron, E. Jeanneau, C. Thieuleux and C. Camp, *Inorg. Chem.*, 2022, **61**, 5715–5730.
41 Y. Takenaka and Z. Hou, *Organometallics*, 2009, **28**, 5196–5203.
42 S. Lassalle, R. Jabbour, I. Del Rosal, L. Maron, E. Fonda, L. Veyre, D. Gajan, A. Lesage, C. Thieuleux and C. Camp, *Journal of Catalysis*, 2020, **392**, 287–301.
43 S. Lassalle, J. Petit, R. L. Falconer, V. Hérault, E. Jeanneau, C. Thieuleux and C. Camp, *Organometallics*, 2022, **41**, 1675–1687.
44 J. Riedhammer, J. R. Aguilar-Calderón, M. Miehlich, D. P. Halter, D. Munz, F. W. Heinemann, S. Fortier, K. Meyer and D. J. Mindiola, *Inorg. Chem.*, 2020, **59**, 2443–2449.
45 S. T. Löffler, J. Hümmer, A. Scheurer, F. W. Heinemann and K. Meyer, *Chem. Sci.*, 2022, **13**, 11341–11351.
46 K. G. Moloy and T. J. Marks, *Inorganica Chimica Acta*, 1985, **110**, 127–131.
47 J. A. Higgins, F. G. N. Cloke and S. M. Roe, *Organometallics*, 2013, **32**, 5244–5252.

The experimental and computational data associated with this article are provided in the ESI.